Timing of rifting in the Alboran Sea basin — correlation of borehole (ODP Leg 161 and Andalucia A-1) to seismic reflection data: implications for basin formation

Kush Tandon [a,*], Juan M. Lorenzo [a,1], Joaquin de La Linde Rubio [b,2]

[a] Department of Geology and Geophysics, Louisiana State University, Baton Rouge, LA 70803-4101, USA
[b] Instituto Andaluz de Ciencias de Tierra, C.S.I.C. and University of Granada, Granada, 18071, Spain

Abstract

To constrain the timing of rifting in the western, eastern, and northern parts of the Alboran Sea basin, seismic reflectors, corresponding to biostratigraphic boundaries and unconformities from the Miocene to Recent, are correlated using synthetic seismograms. Regions of adjacent coeval compression and extension are found in the Alboran Sea basin. Normal faulting continues in parts of the eastern Alboran Sea basin later than in the western Alboran Sea basin. Seismic reflection data in the vicinity of ODP Site 976 (western Alboran Sea basin) suggest that rifting ended in the Miocene. Near Site 976 (western Alboran Sea basin), no compressional features affect Miocene and younger sediments. In the eastern Alboran Sea basin north of Al-Mansour Seamount (ODP Site 977), normal faults are observed in Miocene and Early Pliocene sediments. Later folds affect Pleistocene–Recent sediments in the eastern Alboran Sea basin (Site 977). After the folding event, there is evidence for normal faulting in Pleistocene–Recent sediments close to Site 977. South of Al-Mansour Seamount (ODP Site 978), compressional features in the eastern Alboran Sea basin from Miocene to Recent are evidenced by reverse faulting followed by folding. In the northern Alboran Sea basin (Andalucia A-1 well), there is evidence for strike-slip faulting in the Late Miocene that can be related to the Serrata fault system. We envision the development of the Alboran Sea basin through a southeasterly migration of the delaminating continental lithosphere to explain younger extension in the eastern Alboran Sea basin. The rate of the migration of the delamination front is of the range of millimeters–centimeters/year. We see evidence for the migration of the delamination front from Miocene to Recent as tectonic inversion occurs near Site 977. In contradiction to an extensional collapse hypothesis for the formation of the Alboran Sea, rifting did not end in the Late Miocene in the entire Alboran Sea basin. We exclude retreating subduction in a westward direction or a westward continental delamination as a model for Alboran Sea basin development because it would predict younger extension in the western part of the basin. © 1998 Elsevier Science B.V.

Keywords: Alboran Sea; basin formation; continental rifting; delamination; ODP; synthetic seismograms

Corresponding author. Fax: + 1 504 388 2302. E-mail: kush@gypsum.geol.lsu.edu
[1] E-mail: juan@tellus.geol.lsu.edu. Fax: + 1 504 388 2302.
[2] E-mail: jlinde@goliat.ugr.es. Fax: + 34 58 243384.

1. Introduction

One of the key objectives of Ocean Drilling Program (ODP) Leg 161 (May–July 1995) in the western Mediterranean was to explain the formation of the Alboran Sea extensional basin (Comas et al., 1996). This basin subsided contemporaneously with a mountain building event at its outer flanks, in the Betics of Spain and in the Rif of Africa (Platt and Vissers, 1989; Maldonado and Comas, 1992; Comas et al., 1996). Study of Alboran Sea basin helps understand the development of analogous continental extensional basins in general in the Mediterranean Sea region including the northern Tyrrhenian Sea basin and the Pannonian basin (Watts et al., 1993).

Extensional faulting patterns in the Alboran Sea region may be the result of collapse of a thickened lithosphere caused by the convergence between Africa and Eurasia in the N–S to NW–SE direction (Dewey, 1988; Platt and Vissers, 1989). An extensional collapse model predicts an E–W subsidence where the timing of extension is synchronous throughout the Alboran Sea basin (Docherty and Banda, 1995). Other mechanisms proposed for the Miocene extension include mantle delamination (Bird, 1979; Channell and Mareschal, 1989; Docherty and Banda, 1995; Comas et al., 1996; Seber et al., 1996) and back-arc extension in a narrow, rapidly retreating subduction zone (Malinverno and Ryan, 1986; Zeck et al., 1992; Royden, 1993). In addition, Maldonado et al. (1992) propose that sub-basins of the Alboran Sea are created by dextral shear, tectonic escape, or pull-apart basins due to the northwest–southeast convergence between Africa and Eurasia from the Miocene onward. De Larouziere et al. (1988) also propose that the entire Alboran Sea basin tectonics is dominated by a group of sinistral strike-slip faults termed as 'Trans-Alboran shear zone'. These hypotheses predict that the timing of extension is not uniform throughout the basin. Using mostly industry wells in the northern Alboran Sea to conduct regional 2D backstripping, Docherty and Banda (1995) show that the basin opened in an E-to-SE direction.

The precise period when the main rifting event in the Alboran Sea basin took place is not known

(Watts et al., 1993). Comas et al. (1992) and Watts et al. (1993) propose the following stages of tectonic evolution for the Alboran Sea: (1) initial rifting during Aquitanian–Burdigalian, (2) major rifting lasting through Langhian–Tortonian, (3) basin shortening in the Upper Tortonian/Messinian to Recent. One of the aims of this study is to verify the ages of the stages put forth by Comas et al. (1992) and Watts et al. (1993) by dating the extensional features identified on seismic reflection data. We also test whether the cessation of the rifting throughout the Alboran Sea basin is uniform or not by examining the seismic reflection data from different parts of the basin. Also, we want to investigate the role of the Serrata fault system in the development of the northern Alboran Sea basin in the Late Miocene (De Larouziere et al., 1988; Watts et al., 1993). The Serrata fault system consists of a series of sinistral strike-slip faults originating onshore from the Betic transcurrent shear zone (Woodside and Maldonado, 1992) and is considered to be a part of the 'Trans-Alboran shear zone' (De Larouziere et al., 1988), as shown in Fig. 1.

Synthetic seismograms are used to tie the well depths and biostratigraphic data with the key seismic stratigraphic sequences and their bounding unconformities using laboratory physical properties and wireline logging from ODP Leg 161 and the Andalucia A-1 well. ODP Sites 976 (Fig. 2), 977, and 978 (Fig. 3) and an Elf Aquitaine well, Andalucia A-1 (Fig. 4) are located in different sub-basins within the Alboran Sea basin (Fig. 1). These synthetic seismograms are used to tie well depths and biostratigraphic data to the single-channel seismic reflection data from ODP Leg 161 (Comas et al., 1996) and multi-channel seismic data from R/V *Robert D. Conrad* Cruise RC2911 (Watts et al., 1993) in the Alboran Sea basin (Fig. 1). Fig. 1 shows the location of well sites and seismic survey tracks in the Alboran Sea. Reflectors cannot be correlated between each sub-basin and therefore must be correlated separately for each individual basin for which there are data. This study represents the first non-commercial attempt to correlate seismic and well data using synthetic seismograms in different parts of the Alboran Sea. Synthetic seismograms tie borehole
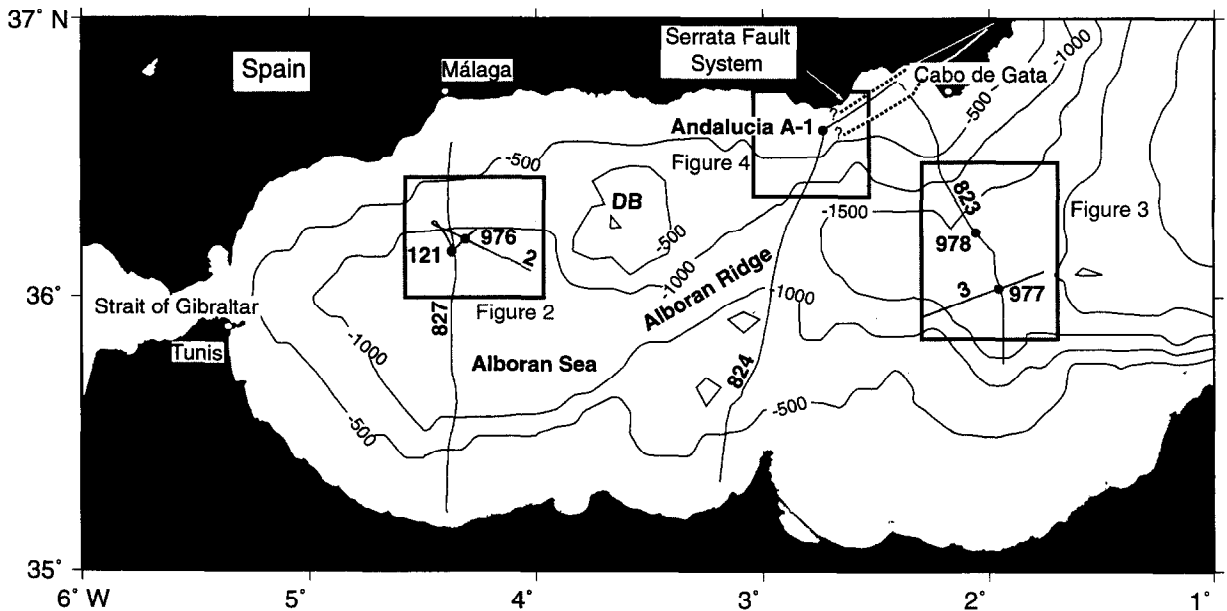
Fig. 1. Bathymetric map for the Alboran Sea contoured at 500 m intervals. Solid lines = ship tracks for ODP Leg 161 underway geophysics and R/V *Robert D. Conrad* survey (Cruise RC2911) used in this study. Lines 2 and 3 belong to ODP Leg 161 single-channel survey and lines 823, 824, and 827 to multi-channel Cruise RC2911. Dots = ODP sites (976, 977, and 978), DSDP site (121) and the industry well, Andalucia A-1. Rectangular regions around the drill sites locate Figs. 2–4. Dashed lines = the inferred continuation of the Serrata fault system offshore. *DB* = Djibouti Bank (Woodside and Maldonado, 1992)

data to seismic reflection surveys more accurately than using averaged travel times or assigning boundaries on the basis of qualitative seismic facies analysis. Synthetic seismograms are developed from laboratory physical properties and borehole logging data which incorporate the changes in these properties to a greater detail. Also, synthetic seismograms allow us to match the wavelet of the synthetics with the seismic reflection data for more accurate correlation. Preliminary biostratigraphic age correlation with seismic reflection data in the vicinity of the ODP drill sites was done on board ODP Leg 161 using averaged travel times (Comas et al., 1996). Jurado and Comas (1992) have carried out a seismic stratigraphy analysis for the northern Alboran Sea basin using only seismic and well log facies analysis.

2. Geological background

The Alboran Sea region straddles a convergent boundary between the African and Eurasian plates (Dewey, 1988; Platt and Vissers, 1989). The Alboran Sea is 1 km deep and contains at least 7 km of Miocene–Recent sediments within several sub-basins (Watts et al., 1993) (Fig. 1). The regional extension of the Alboran Sea basin is manifested by low-angle normal faults observed onshore Spain (Garcia-Dueñas et al., 1989). One of the most prominent bathymetric features in the Alboran Sea basin is the NE–SW trending Alboran Ridge (Watts et al., 1993) (Fig. 1). Beneath the sediments, lies a Paleozoic metamorphic basement within a thinned (18–22 km) continental crust (Platt and Vissers, 1989; Docherty and Banda, 1992). The Miocene–Recent stratigraphic framework for the Alboran Sea basins is developed on the basis of Neogene sedimentary sequences (Aquitanian–Recent) in the Internal Zone of the Betic Cordillera (Fernandez and De Galdeano, 1992; De Galdeano and Vera, 1992) and from commercial exploration (Comas et al., 1992) and ODP wells (Comas et al., 1996) in the Alboran Sea.

At Site 976, where Miocene–Recent sediments are cored, four major unconformities are identified:
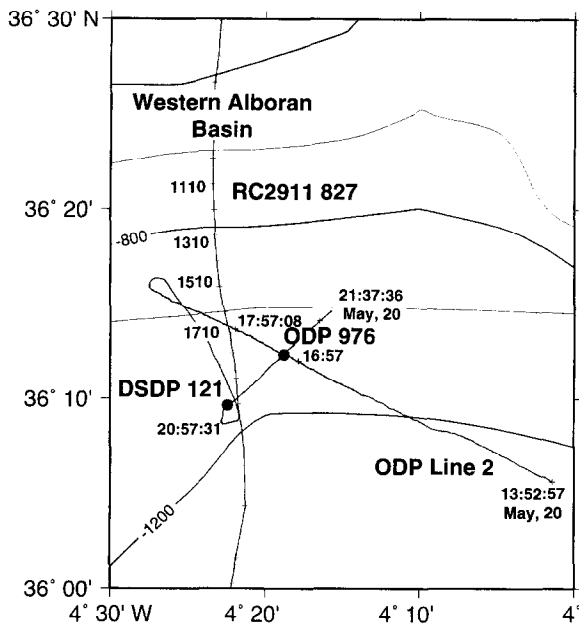
Fig. 2. Location of ODP Site 976 and DSDP Site 121 (dots) and tracks for seismic lines ODP line 2, RC2911 line 827. Cross marks on RC2911 line 827 track occur at 100 CDP (Common Depth Point) intervals. Cross marks on ODP line 2 show GMT navigation time (hour:minute:second). The bathymetric contour interval is 200 m.

(1) metamorphic basement–Serravallian;
(2) within the Late Miocene (intra-Tortonian);
(3) in the Miocene–Early Pliocene (Messinian–Zanclean);
(4) in the Early–Late Pliocene (Zanclean–Piacenzian) (Comas et al., 1996) (Fig. 5).

The three unconformities within the sedimentary section are not detectable from the lithostratigraphy or physical properties alone (Fig. 5), but are determined on the basis of microfossils (Comas et al., 1996). Site 976 does not contain all the unconformities identified by Comas et al. (1992) within the Alboran Sea such as: (1) Aquitanian–Betic basement contact; (2) Burdigalian–Langhian boundary; (3) intra–Upper Serravallian; and (4) Lower Tortonian.

At Site 977 (eastern Alboran Sea basin), an unconformity found in the Lower Pliocene lies approximately at the boundary between lithostratigraphic subunits of intensely to slightly bioturbated nannofossil clays (Comas et al., 1996) (Fig. 6). At Site 978 (eastern Alboran Sea basin), a gravel-

bearing interval in the uppermost Miocene represents a strong erosional surface in the eastern Alboran Sea basin (Comas et al., 1996) (Fig. 7). At Andalucia A-1 (northern Alboran Sea basin), the disconformity between the Miocene sediments and the Betic basement is at 2727 mbsf (Lambert, 1981) (Fig. 8). Identifying different unconformities corresponding to different stages of the Miocene gives us key control on the initiation and the duration of the rifting in the Alboran Sea basin. The Pliocene unconformity gives a control on the later tectonics in the Alboran Sea basin when compression and strike-slip faulting played an important role (Comas et al., 1992; Watts et al., 1993).

3. Data

Bulk density and the compressional-wave velocity of sediments and rocks are the key physical properties used to produce synthetic seismograms. The bulk density and compressional-wave velocity data from shipboard laboratory measurements during ODP Leg 161 and wireline logging data from the Andalucia A-1 well are used to develop the synthetic seismograms.

4. Physical properties

During ODP Leg 161, core recovery was sufficiently high (87%) to allow regular sampling for the construction of synthetic seismograms using shipboard laboratory physical properties. Logging data collected during ODP Leg 161 are too poor in quality to construct synthetic seismograms. ODP Leg 161 sonic logs suffer from cycle skipping and bridges (Comas et al., 1996). Shipboard laboratory physical properties data (wet bulk density and compressional-wave velocity) are measured once every section (~ 1.5 m) or every other section (~ 3.0 m) (Comas et al., 1996). Both sampling intervals are far better than the resolution of the available seismic reflection data and are appropriate for synthetic seismogram modeling. The vertical resolution in seismic reflection data varies from 1/8 to 1/4 of the dominant wavelength of the source wavelet used for the seismic survey (Sheriff, 1977). The peak frequency for ODP underway
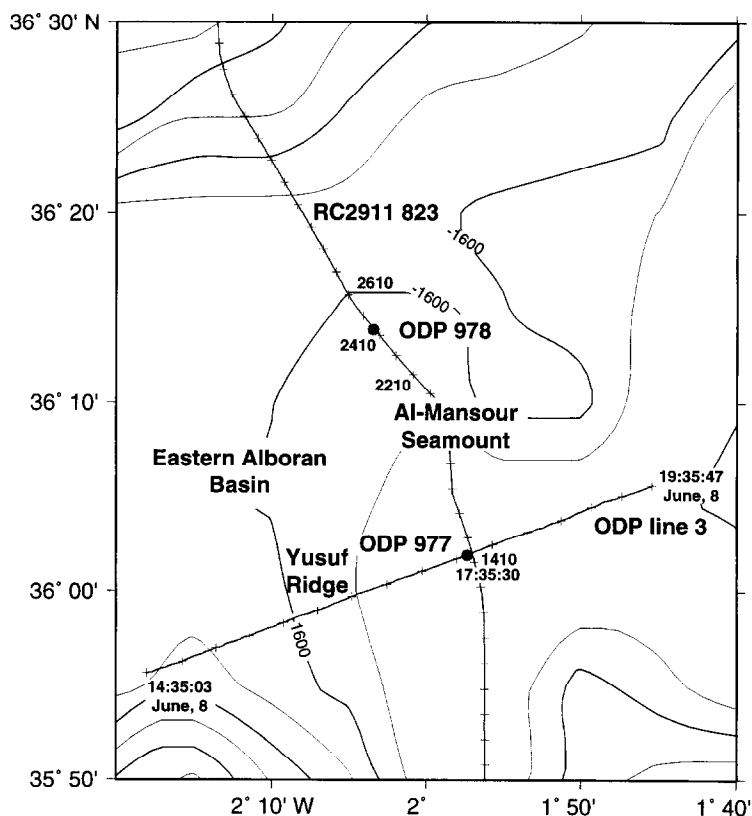
Fig. 3. Location of ODP Sites 977 and 978 (dots) and tracks for seismic lines ODP line 3 and RC2911 line 823. Cross marks on RC2911 line 823 track occur at 100 CDP intervals. Cross marks on ODP line 3 profile show GMT navigation time (hour:minute: second) approximately every 20 min. The bathymetric contour interval is 200 m.

geophysics is around 35 Hz. Using compressional velocities in the range of 1600–2000 m/sec, the vertical resolution of the seismic data varies from 5 to 15 m. The peak frequency for Cruise RC2911 is around 15 Hz. Similarly, the vertical resolution of the RC2911 ranges from 13 to 33 m.

Compressional-wave velocity was measured using the Digital Sound Velocimeter (DSV) for softer sediments and the Hamilton Frame velocity transducer for consolidated sediments (Comas et al., 1996). The quality of laboratory physical properties data in general is good for ODP sites used for modeling. However, for Site 976 the data quality of compressional-wave velocities was degraded in the sediment cores because of gas expansion (Comas et al., 1996). When cores are brought to the surface, methane gas expansion may create microfracturing which can attenuate

the signal required for measuring laboratory velocity values (Lorenzo and Hesselbo, 1996).

There are two limitations in using the laboratory physical properties data for the construction of synthetic seismograms: (1) rebound effect (Hamilton, 1976) and (2) inaccuracies in the compressional-wave velocity measurement (Gregory, 1977). The rebound effect causes a slight decrease in the density, due to increase in the volume of the sediments when cores are brought to the surface (Hamilton, 1976). Laboratory measurements of compressional-wave velocities are slightly lower than in situ measurements of compressional-wave velocities such as wireline logging (Gregory, 1977). Values from laboratory bulk density data from ODP Leg 161 (Figs. 4–7) are comparable to the wireline data from Andalucia A-1 (Fig. 8) for the shallow sedimentary section. Any core disturbance
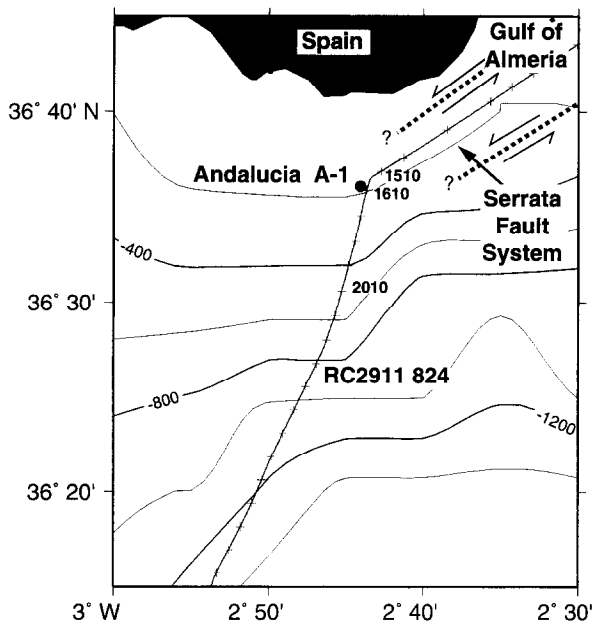
Fig. 4. Location of industry well, Andalucia A-1 and ship tracks for the multi-channel seismic lines RC2911 line 824. Cross marks along RC2911 line 824 profile track occur at 100 CDP intervals. The dashed line shows that the continuation of the Serrata fault system is inferred offshore (Woodside and Maldonado, 1992). The bathymetric contour interval is 200 m.

will cause more scatter than the true velocity section (Wilkens, pers. commun.). A comparison between laboratory physical properties and wire-line logging data from ODP Leg 150 (Lorenzo and Hesselbo, 1996) and other ODP Legs show small variations between them for clay-rich sediments (Wilkens, pers. commun.). We believe that these possible uncertainties do not seriously effect our correlation.

5. Shipboard laboratory physical properties

5.1. Site 976

At Site 976, shipboard laboratory velocity measurements were not made between 90 and 670 mbsf at regular intervals because of gas expansion in the sedimentary section of the core. Also, some unusually high velocities of about 5 km/sec are given by Late Pliocene semi-lithified sands (Comas et al., 1996). However, wet bulk density at regular

intervals is available throughout Site 976. Using bulk density and compressional wave–velocity empirical relationships (Gardner et al., 1974; Hamilton and Bachman, 1982), we developed a velocity profile for the sedimentary section. The velocity profile uses the empirical density–velocity relationships of Hamilton and Bachman (1982) for density values between 1.25 and 2.10 gm/cc and the relation of Gardner et al. (1974) for density values outside the 1.25–2.10 gm/cc range. The derived velocity profile for sediments is then concatenated with the shipboard laboratory velocity measurements from the metamorphic basement (Fig. 5).

5.2. Sites 977 and 978

At Site 977, both the laboratory wet bulk density and compressional-wave velocity measurements collected shipboard are of adequate quality (Comas et al., 1996) to be used for synthetic seismogram generation (Fig. 6). At Site 978, continuous coring was carried out for the shallowest 213 mbsf (Comas et al., 1996). In order to cover a gap in physical properties for Late Pliocene–Pleistocene nannofossil clays, physical properties data from Site 977 (Fig. 6) are merged with those of Site 978 (Fig. 7). Site 978 lies within the same 35 km wide graben as Site 977 but is separated by the Al-Mansour Seamount (Comas et al., 1996), as shown in Fig. 3. Poor core recovery at the late Late Miocene–Early Pliocene boundary creates an abrupt transition in the physical properties between the Pliocene and late Late Miocene (Fig. 7).

6. Wireline logging

6.1. Andalucia A-1

Andalucia A-1 well (258.0–2890.75 mbsf) was completely logged with a sonic tool in the Miocene–Pliocene section but density logs were taken only in Lower Miocene sediments. A density profile (Fig. 8) has been developed for the entire Andalucia A-1 well from the sonic logs using an empirical relationship (Gardner et al., 1974).

In order to complete the shallowest section of sonic log at Andalucia A-1 well, we merged the
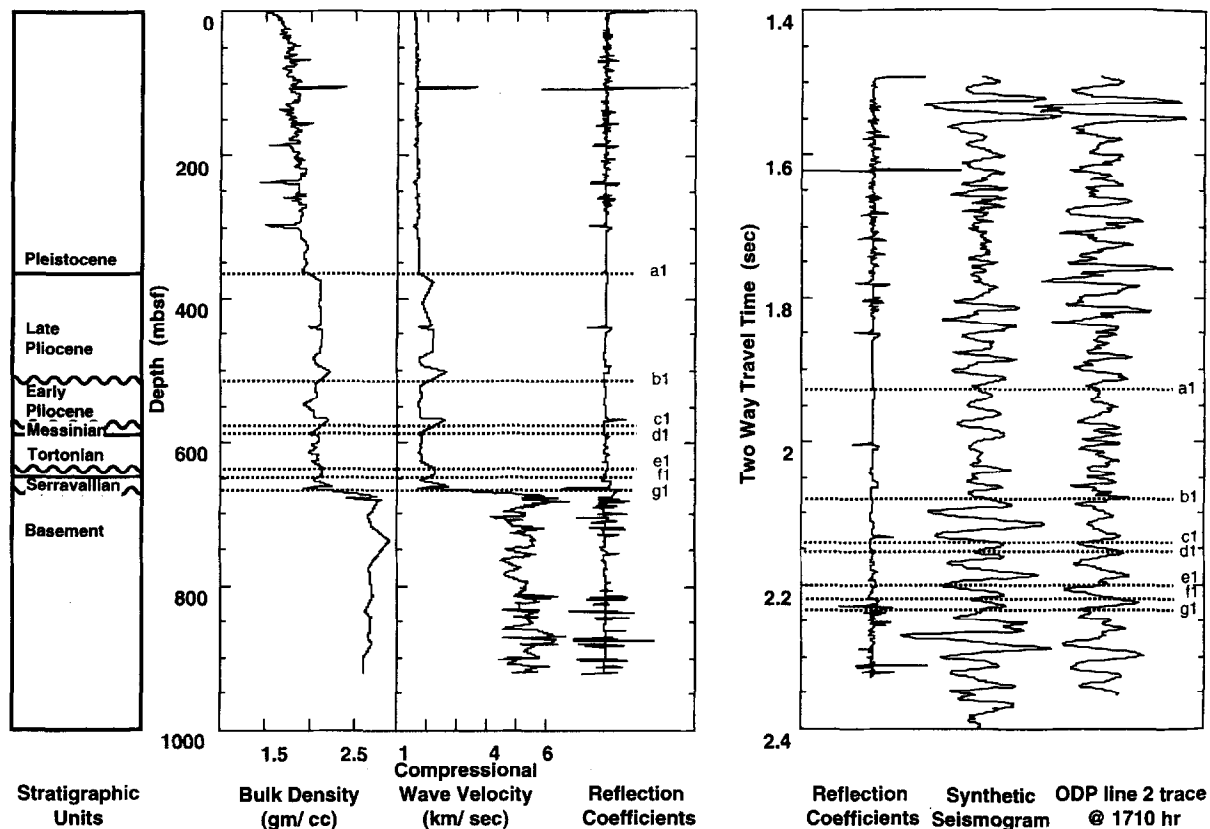
ODP 976 and line 2 @ 1710 hr

Fig. 5. Correlation between the synthetic seismograms developed from Site 976 and ODP line 2.

sonic log of ODP Site 976 from 73.3–258.0 mbsf. Merging the logs is valid in this case because both Site 976 (Comas et al., 1996) and Andalucia A-1 well (Lambert, 1981) contain Late Pliocene–Pleistocene, nannofossil-rich clays in this section. These sediments have a similar age, composition, and probably the same physical properties.

7. Seismic reflection data

bn   Seismic data used for correlation was taken from the single-channel seismic surveys of ODP Leg 161 and multi-channel seismic surveys of R/V *Robert D. Conrad* Cruise RC2911 (Watts et al., 1993) (Figs. 9–12). Most of the single-channel seismic survey for ODP Leg 161 used a 80 in³

water gun (Comas et al., 1996). However, a 200 in³ water gun was used in the NE–SW direction of the seismic line which passes through Site 976 (Fig. 2) to image more clearly the deeper portion of the basin on the either side of the basement ridge (Comas et al., 1996). The multi-channel seismic Cruise RC2911 employed a 5346 in³ BOLT air gun array as a source.

8. Methods

8.1. Synthetic seismogram modeling

We used a linear convolution filtering approach for synthetic seismogram modeling (Peterson et al., 1955). Contrasts in the acoustic impedance (bulk
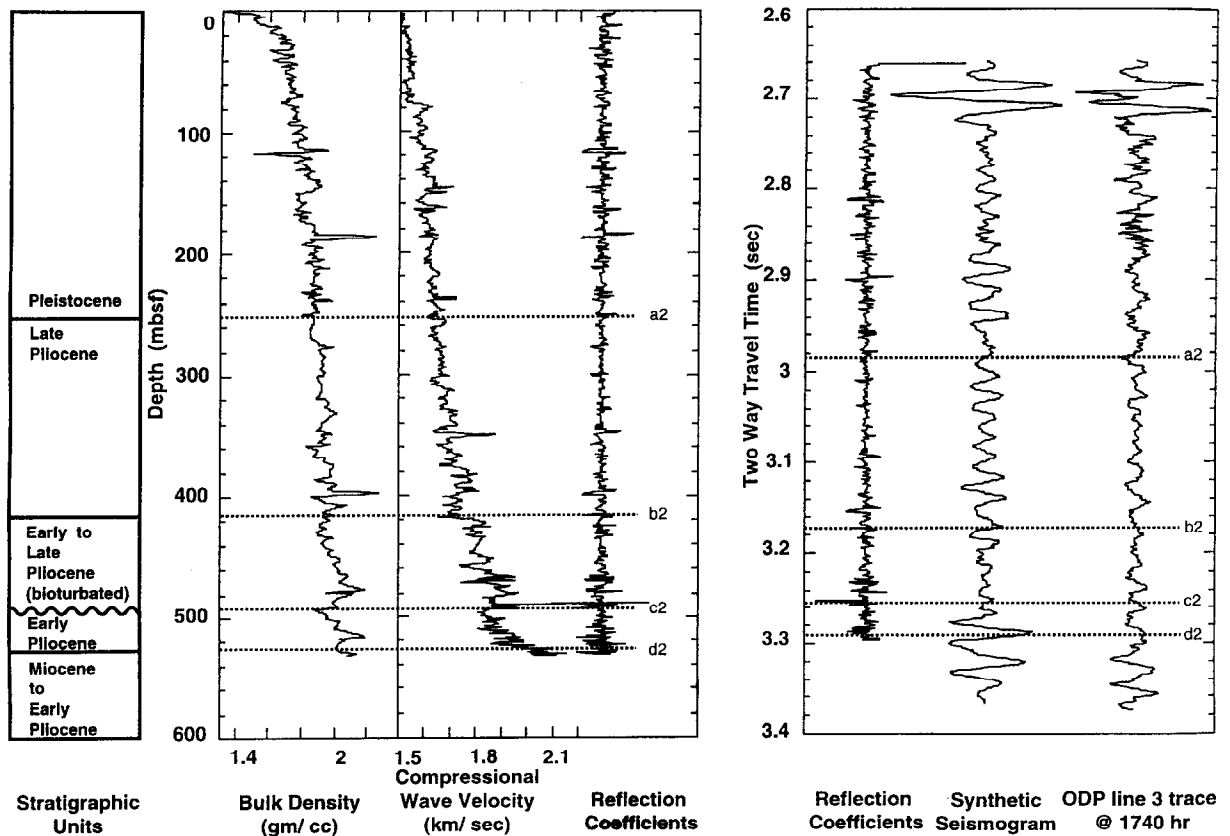
ODP 977 and line 3 @ 1740 hr

Fig. 6. Correlation of synthetic seismograms developed from ODP 977 to ODP line 3.

density × compressional-wave velocity) of the earth establish boundaries capable of producing normal incidence reflections (Sheriff, 1981). The reflection coefficient series produced by acoustic impedance contrasts were convolved with an estimated source wavelet to produce a synthetic seismogram (Sheriff, 1981). The linear convolution filter approach does not take into account the effects of sea bottom multiples, internal multiples or geometric spreading. However, the linear convolution approach provides a very good time estimate for primary arrivals in a horizontally layered earth. Most of the sediments in the vicinity of our drill sites (ODP Sites 976, 977, 978, and Andalucia A-1 well) are horizontal. The linear convolution technique for generating synthetic seismograms serves

the purpose of correlating primary arrivals on the seismic reflection data.

The accuracy of the well-to-seismic correlation also depends on estimating an appropriate source wavelet. We approximated the far-field source wavelet by using part of the sea floor reflection on a horizontal topography at deep water depths. Different source wavelets were picked for the 80 in^3 water gun source, the 200 in^3 water gun source from the ODP 161 underway geophysics, and a source for Cruise RC2911. Data from ODP sites were resampled at 0.5 m and from Andalucia A-1 at 2.0 m to produce synthetic seismogram models. The spatial resampling is an order of magnitude finer than the resolution of the seismic data used for this study. The time sampling for the synthetic
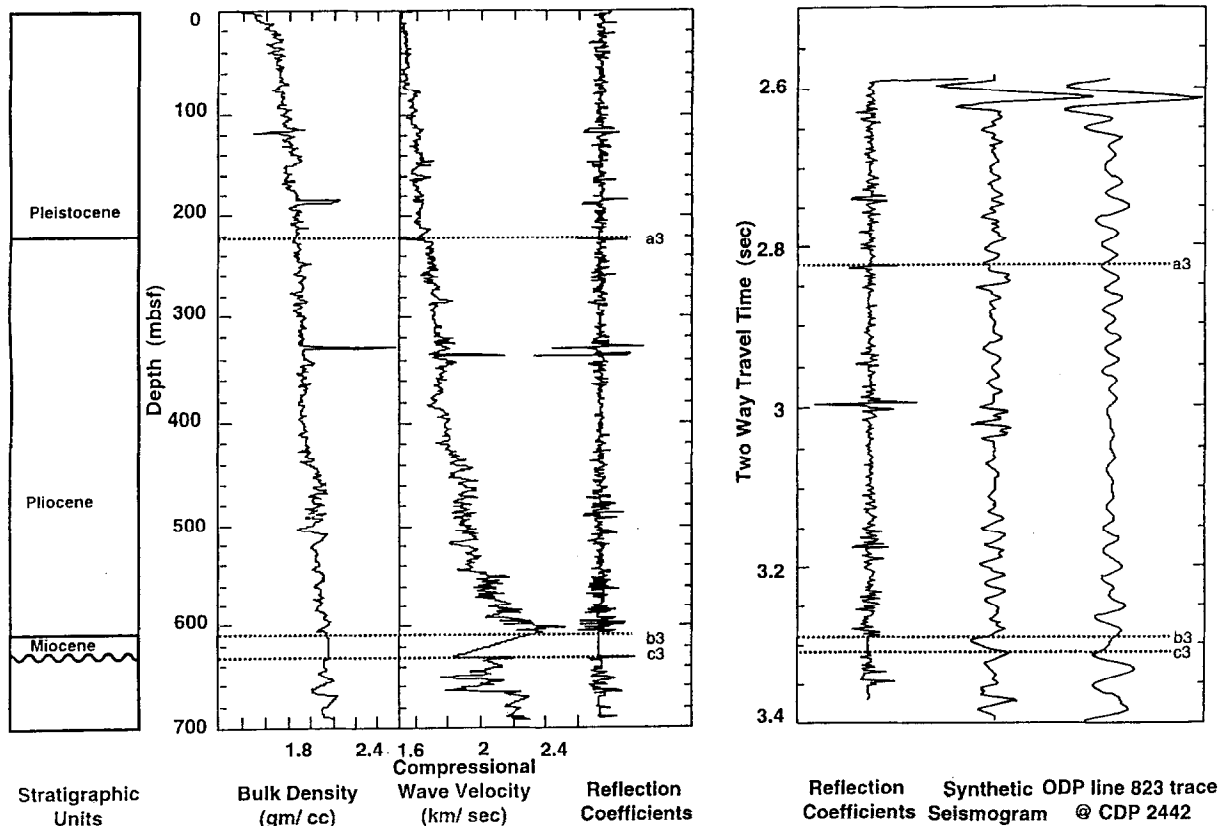
ODP 978 and line 823 @ CDP 2442

Fig. 7. Correlation between the synthetic seismograms developed from ODP 978 and the RC2911 line 823.

seismogram modeling was at 1 msec for correlation to single-channel surveys and 2 msec for the multi-channel surveys. The depth and time sampling for the synthetic seismogram modeling is fine enough to delineate features required for well-to-seismic correlation.

8.2. Well-to-seismic correlation

Three steps are followed in well-to-seismic correlation. The first step identifies the key geological boundaries in the well. In our case we chose to tie biostratigraphic boundaries and unconformities in the borehole data with the seismic reflection surveys. In the second step, these boundaries are identified in the reflection coefficient series computed as a function of depth and then pattern matched to the reflection coefficient series with respect to time. There is a one-to-one correspondence between the reflection coefficient series in time and the synthetic seismograms. In the final step, the pulse in the synthetic seismograms is matched with the seismic reflection data. Since our technique for developing synthetic seismograms does not account for attenuation of the wave energy, the well-to-seismic correlation is limited to peak-to-peak matching. We do not compare the amplitude between the synthetic seismograms and the seismic trace.

Andalucia A-1 well is situated 697 m west of CDP (Common Depth Point) 1610 on RC2911 line 824 (Fig. 4). At all wells (Figs. 5–7) except Andalucia A-1 (Fig. 8), we positioned the synthetic seismogram with respect to the sea floor.
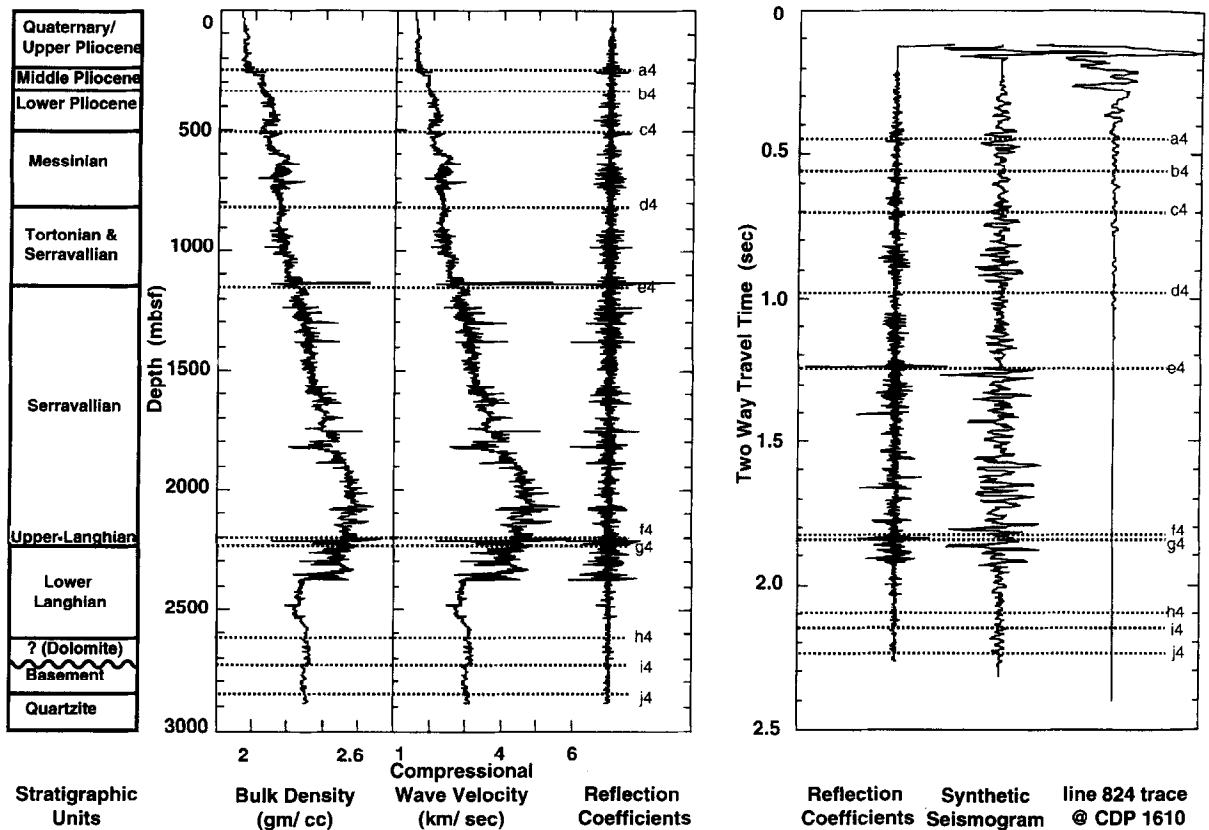
Andalucia A-1 and RC2911 line 824 @ CDP 1610

Fig. 8. Correlation between the synthetic seismograms developed from Andalucia A-1 well and the RC2911 line 824.

The shallow sea floor reflectors on RC2911 line 824 in the vicinity of Andalucia A-1 well (the sea bottom is 92 m deep) are not created in conditions of normal incidence. This is because the sea floor depth is comparable to the narrower source–receiver offset. Therefore, the synthetic seismogram generated at Andalucia A-1 is referenced to a deeper reflector positioned at 0.3 sec (Fig. 8).

9. Key reflectors

Reflectors corresponding to different stages in the Miocene as well as the boundaries for the Pliocene and Pleistocene are identified. Identification of these reflectors can help time the

cessation of extension and inception of compressional features in different parts of the Alboran Sea basin. The position of the reflectors for different locations (Sites 976, 977, 978, and Andalucia A-1) corresponding to biostratigraphic data are presented in Table 1.

9.1. Site 976

On ODP line 2 (Fig. 9), seven reflectors from Betic (Paleozoic) basement to Recent are correlated on the basis of synthetic seismograms developed from Site 976 (Fig. 5). Reflectors 'g1' (Metamorphic basement–Serravallian), 'e1' (intra-Tortonian), 'c1' (Messinian–Zanclean boundary), and 'b1' (Zanclean–Piacenzian boundary) appear
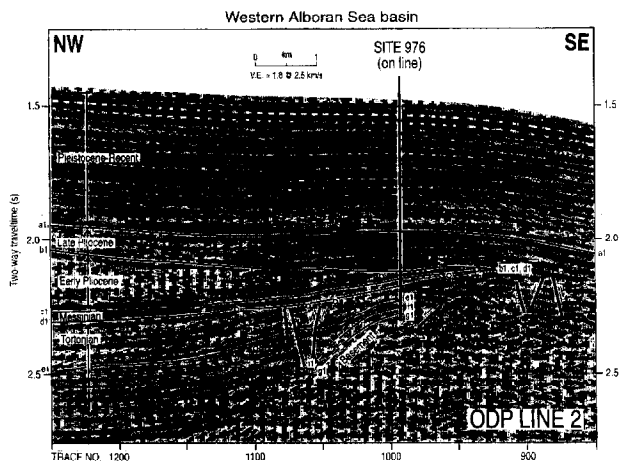
Fig. 9. Seismic stratigraphic and structural interpretation super-imposed on ODP line 2. Intersection of ODP Site 976 is marked by vertical line. The letters used for well-to-seismic correlation are defined in Fig. 5 and Table 1. A 48 msec time delay in the raw seismic reflection ODP line 2 has been removed. The circles point to the seismic truncations. Arrows indicate inferred fault movement.
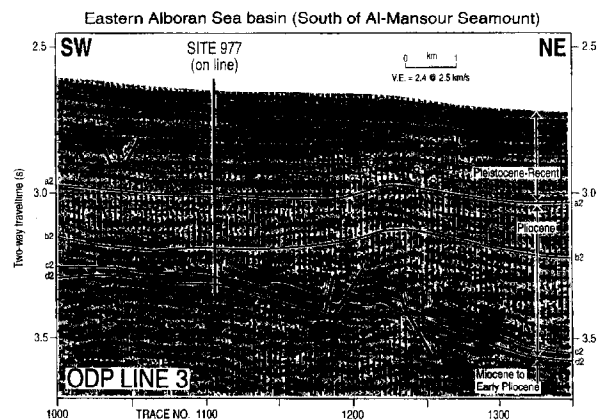
Fig. 10. Seismic stratigraphic and structural interpretation superimposed on ODP line 3. Intersection of ODP Site 977 and RC2911 line 823 is marked with vertical lines. The letters used for well-to-seismic correlation are defined in Fig. 6 and Table 1. A 24 msec time delay in the raw seismic reflection ODP line 3 has been removed. The circles point to the seismic truncations. Arrows indicate inferred fault movement.

as borehole unconformities (Comas et al., 1996). Reflectors 'b1', 'c1' and 'd1' onlap a horst and truncate underlying reflectors (Fig. 9). The horst displays a highly diffractive top surface due to faults (Comas et al., 1996), as shown in Fig. 9. The thin Miocene sedimentary section at ODP Site 976 and DSDP 121 (Fig. 2) is considered evidence that the horst was a morphological high during most of the Miocene (Watts et al., 1993; Comas et al., 1996). These unconformities are regional in the western Alboran Sea basin as they can also be observed along RC2911 line 827 (Fig. 2). At Site 976, the well-to-seismic correlation using synthetic seismograms agrees rather well with the prelimi-nary shipboard correlation presented by Comas et al. (1996).

9.2. Sites 977 and 978

Correlation of Site 977 (Fig. 6) with ODP line 3 identifies four reflectors from the uppermost Miocene–Pleistocene (Fig. 10). Reflector 'c2' cor-responds to a borehole unconformity within the Early Pliocene (Fig. 6). Near traces 1200–1250, reflectors above 'c2' are curved and onlapped by overlying Pleistocene–Recent reflectors (Fig. 10).

Three key reflectors from the uppermost Miocene–Pleistocene are discerned along RC2911 line 823 (Fig. 11) using Site 978 (Fig. 7). Pliocene reflectors (between 'b3' and 'a3') show a mounded pattern and toplap the reflectors above them (Fig. 11). There is a clear distinction between the pattern of reflectors within the Miocene section and Pliocene–Pleistocene section (Figs. 10 and 11). The reflectors corresponding to the Miocene are diffractive in nature whereas the Pliocene Pleistocene section shows parallel reflectors (Figs. 10 and 11). Our well-to-seismic correlations are more detailed at Sites 977 and 978 than those presented in the initial reports (Comas et al., 1996). This boundary helps us understand the neotecton-ics of the eastern Alboran Sea basin in a more precise manner (Figs. 10 and 11).

9.3. Andalucia A-1

Ten biostratigraphic boundaries (Fig. 8) are identified from Andalucia A-1. Only four of these boundaries are correlated to reflectors on RC2911 line 824 (reflectors 'a4', 'b4', 'c4', and 'd4' in Fig. 12) due to inadequate data quality beneath 1.5 sec. The borehole report for Andalucia A-1 does not give details regarding the unconformities

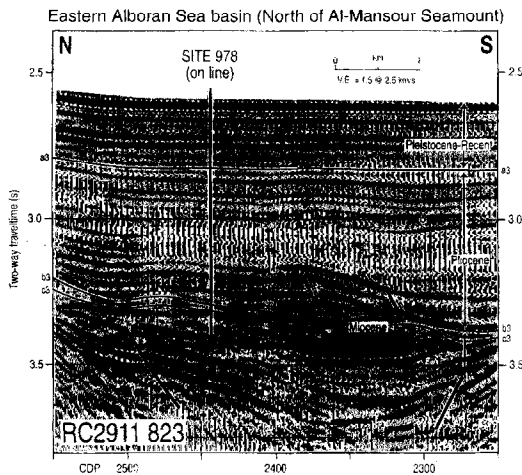Eastern Alboran Sea basin (North of Al-Mansour Seamount)

Fig. 11. Seismic stratigraphic and structural interpretation superimposed on RC2911 line 823. Intersection of ODP Site 978 is marked with a vertical line. The letters used for well-to-seismic correlation are defined in Fig. 7 and Table 1. A 61 msec time delay in the RC2911 line 823 has been removed. The circles point to the seismic truncations. Arrows indicate inferred fault movement.

in the sedimentary section (Lambert, 1981). In Fig. 12, some of the reflectors between 'c4' and 'd4' (Messinian section) show toplapping termination. A toplap can be indicative of a nondepositional hiatus (Mitchum et al., 1977). The results of the synthetic seismogram modeling from Andalucia A-1 well here have changed the position of the reflectors corresponding to the biostratigraphic boundaries determined on the basis of averaged travel times (Lambert, 1981). The position of the reflectors corresponding to different biostratigraphic boundaries picked by us (Table 1) are lower than the ones picked by Lambert (1981). This affects the timing of the structural features in the northern Alboran Sea basin.

10. Discussion

10.1. Western Alboran Sea basin

Normal faulting ends near and below the Miocene–Pliocene boundary (reflector 'd1') on ODP Leg 161 line 2 (Fig. 9). This is consistent with the tectonic evolution proposed by other

workers (Comas et al., 1992; Watts et al., 1993; Chalouan et al., 1997) for the western Alboran Sea basin. However, we do not see any of the post-Miocene compressional features predicted by Comas et al. (1992) or basin-wide strike-slip faulting (De Larouziere et al., 1988; Watts et al., 1993) in Fig. 9 or in the portion of the ODP Leg 161 line 2 not shown. Bourgois et al. (1992) and Campillo et al. (1992), using seismic reflection data from various parts of the western Alboran Sea basin, suggest that the western Alboran Sea basin underwent extension in the Burdigalian–Langhian and then transpression from the Tortonian onward. Such an observation can be explained by the change in maximum principal stress axes between Africa and Eurasia from NW–SE in the Tortonian to N–S in the Late Tortonian to Mid-Pliocene and then to NNW–SSE from the Mid-Pliocene to Quaternary (Montenat et al., 1987), causing rotation of small crustal blocks.

10.2. Eastern Alboran Sea basin

In the eastern Alboran Sea basin, a different tectonic evolution is observed north and south of Al-Mansour Seamount (Fig. 3), as shown in Figs. 10 and 11. South of the Al-Mansour Seamount (Fig. 3), ODP line 3 shows normal faulting in Miocene–Early Pliocene sediments (Fig. 10). North of Al-Mansour Seamount, near Site 978 (Fig. 3), the Miocene–Early Pliocene section displays evidence for reverse faulting (Fig. 11). The presence of reverse faulting agrees with Maldonado et al. (1992) and Woodside and Maldonado (1992) but disagrees with the interpretation by Mauffret et al. (1987). Compression in Pliocene–Pleistocene times in the eastern Alboran Sea basin is evident in terms of folding both near Site 977 (Fig. 10) and Site 978 (Fig. 11). Near Site 977, extensional faulting overlies folds in Pleistocene–Recent sediments (Fig. 10). The sequence of events in the Early Pliocene–Recent near Site 977 (Fig. 10) could be as follows: (1) folding of Early Pliocene sediments, (2) sedimentary onlap of folded structure, (3) normal faulting. In another study of the sub-basins in the eastern Alboran Sea, Woodside and Maldonado

Table 1
Key boundaries in meters below sea floor (mbsf) from ODP Sites 976, 977, and 978 and Andalucia A-1 well and their corresponding seconds below sea floor (sbsf) on the synthetic seismograms

Boundary	Type	Borehole depth (mbsf)	Synthetic seismograms (sbsf)
Site 976			
a1 (Late Pliocene–Recent)	Biostratigraphic	357.92–361.01	0.43
b1 (Early Pliocene–Late Pliocene)	Unconformity	515.10	0.59
c1 (Messinian–Early Pliocene)	Unconformity	573.24	0.65
d1 (Tortonian–Messinian)	Biostratigraphic	587.79	0.67
e1 (intra-Tortonian unconformity)	Unconformity	639.11	0.71
f1 (Serravallian–Tortonian)	Biostratigraphic	650.93	0.72
g1 (Basement–Serravallian)	Unconformity	669.7	0.74
Site 977			
a2 (Late Pliocene–Recent)	Biostratigraphic	417.4	0.33
b2 (Early to Late Pliocene–Late Pliocene)	Biostratigraphic	490.8	0.51
c2 (Early Pliocene–Early to Late Pliocene)	Unconformity	532.9	0.59
d2 (Miocene to Early Pliocene–Early Pliocene)	Biostratigraphic	598.5	0.63
Site 978			
a3 (Pliocene–Recent)	Biostratigraphic	222.77–223.35	0.23
b3 (Miocene–Pliocene)	Biostratigraphic	607.51–611.39	0.70
c3 (Late Miocene unconformity)	Unconformity	620.9	0.72
Andalucia A-1			
a4 (Middle Pliocene–Recent)	Biostratigraphic	268	0.33
b4 (Lower Pliocene–Middle Pliocene)	Biostratigraphic	359	0.45
c4 (Messinian–Lower Pliocene)	Biostratigraphic	508	0.58
d4 (Tortonian and Serravallian–Messinian)	Biostratigraphic	823	0.86
e4 (Serravallian–Tortonian and Serravallian)	Biostratigraphic	1148	1.12
f4 (Upper Langhian–Serravallian)	Biostratigraphic	2206	1.72
g4 (Lower Langhian–Upper Langhian)	Biostratigraphic	2237	1.73
h4 (?(Dolomite)–Lower Langhian)	Biostratigraphic	2633	1.98
i4 (Basement–?(Dolomite))	Disconformity	2727	2.03
j4 (Quartzite–Basement)	Biostratigraphic	2913	2.12

(1992) also describe Recent compressional faulting and strike-slip related activity in the seismic reflection data.

10.3. Northern Alboran Sea basin

We use the development of the Serrata fault system as a means of investigating the possibility of the 'Trans-Alboran shear zone' extending from Spain to the northern Alboran Sea (De Larouziere et al., 1988). Strike-slip faulting can show up as 'flower structures' on reflection seismic data (Biddle and Christie-Blick, 1989). Flower structures extending into Messinian-age sediments and possibly related to movement of the Serrata fault system can be seen in Fig. 12. Our imaging of the flower structure is not clear but we can see steeply

dipping faults ($\sim 60°$) with an apparent change in the slip direction along the inferred faults (Fig. 12). We see strike-slip related activity on Fig. 12, although the Serrata fault system disappears along the coast (Woodside and Maldonado, 1992). Vertical offsets, assumed to be related to the Serrata fault system offshore, are also seen on Spanish surveys south to the portion covered by Fig. 12 (Woodside and Maldonado, 1992). Evidence for the continuation of the Serrata fault system is also seen in the bathymetry in northern Alboran Sea as a development of a canyon system (Woodside and Maldonado, 1992). Fig. 12 confirms the role of the 'Trans-Alboran shear zone' in the Late Miocene, at least in the northern Alboran Sea basin, as proposed by De Larouziere et al. (1988). Strike-slip faulting and formation of
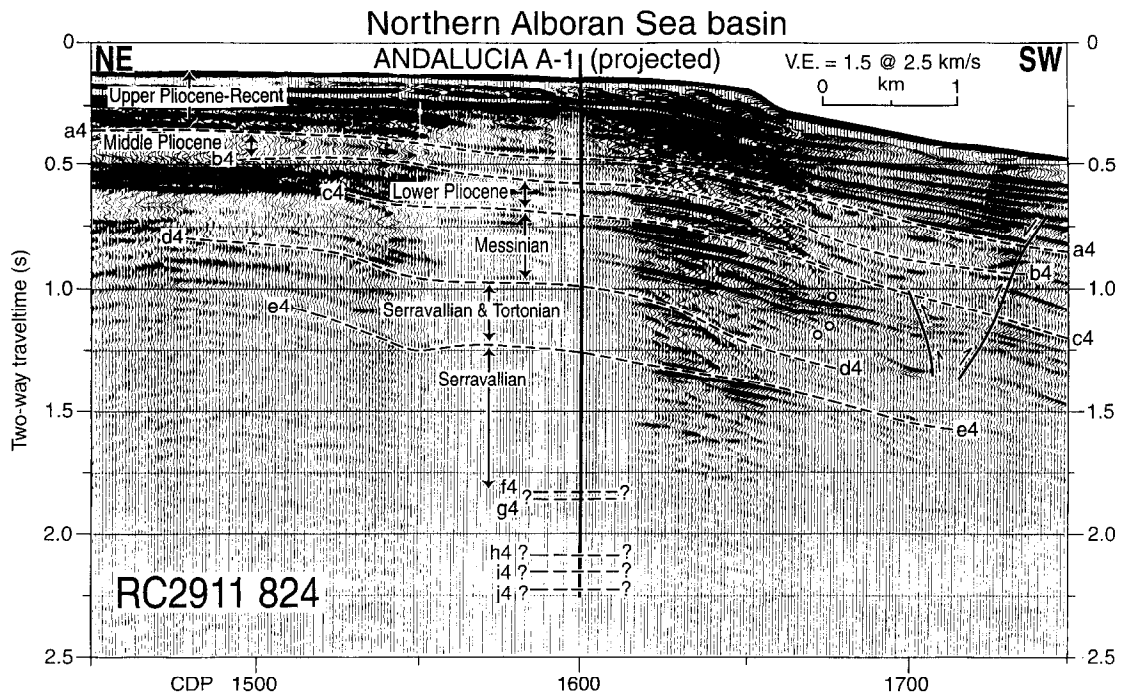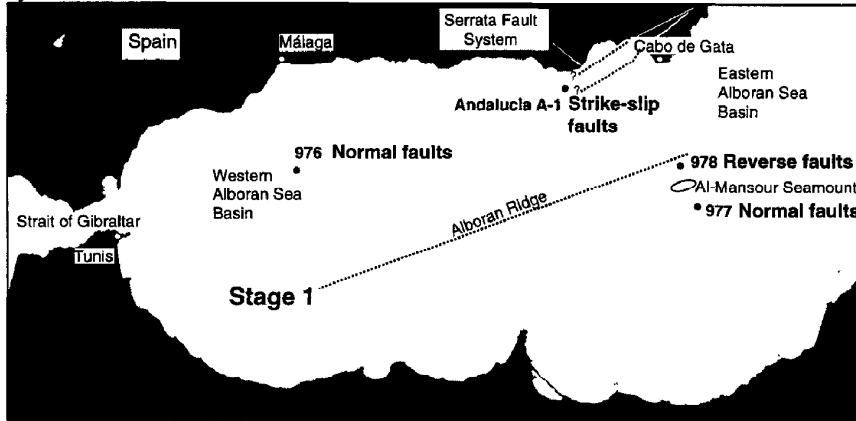
Fig. 12. Seismic stratigraphic and structural interpretation superimposed on RC2911 line 824. Projected Andalucia A-1 well site is marked with vertical line. The letters used for well-to-seismic correlation are defined in Fig. 8 and Table 1. The dashed lines show that the interpretation on RC2911 line 824 is tentative. The circles point to the seismic truncations. The arrows indicate the inferred fault movement.

pull-apart sub-basins have definitely played an important role in Alboran Sea basin neotectonics (Comas et al., 1992; Maldonado et al., 1992; Watts et al., 1993). However, the key question still remains unanswered: whether the strike-slip faulting has only reorganized the Alboran Sea sub-basins since the Late Miocene onwards or has played a key role in the formation of the Alboran Sea basin (De Larouziere et al., 1988; Comas et al., 1992; Maldonado et al., 1992; Watts et al., 1993).
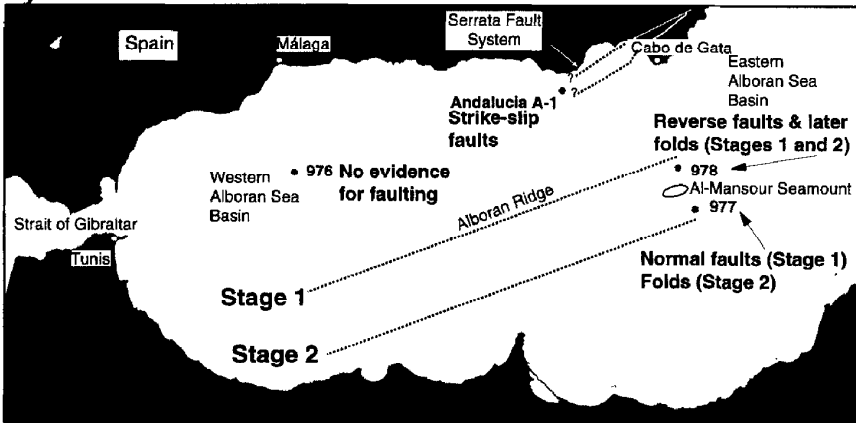
The entire Alboran Sea basin does not comply with the stages of tectonic evolution set by Comas et al. (1992) and Watts et al. (1993). We notice an eastward migration of extension in the Alboran Sea basin in which normal faulting ends in the eastern Alboran Sea basin later than in the western Alboran Sea basin (Fig. 13). This agrees well with the conclusions by Docherty and Banda (1995) that the locus of subsidence in the Alboran Sea basin has moved in an E-to-SE direction. Docherty and Banda (1995) also point out that the total

tectonic subsidence in the western Alboran Sea basin is greater than in the eastern Alboran Sea basin. Our preferred model is that the eastward or southeastward migration of extension in the Alboran Sea basin is through the delamination of lithosphere in an easterly to southeasterly direction which started in the western Alboran Sea basin (Docherty and Banda, 1995), as shown in Fig. 14. The hypothesis of Docherty and Banda (1995) is that in the Middle to Late Miocene the axis along the Alboran Ridge was under compression (Fig. 13a). As the locus of delamination migrated southeast, the Alboran Ridge and the eastern Alboran Basin started to undergo extension (Docherty and Banda, 1995). Channell and Mareschal (1989) predict that the delamination causes adjacent regions of compression and extension (Fig. 14), as seen in the results (Fig. 13). The maximum extension would be on the delaminating side of the lithosphere and shortening would take place in the vicinity where delamination is actually

a) Miocene

Spain Málaga

Serrata Fault System

Cabo de Gata

Eastern Alboran Sea Basin

Andalucia A-1 Strike-slip faults

976 Normal faults

Western Alboran Sea Basin

Strait of Gibraltar

Tunis

Alboran Ridge

978 Reverse faults
Al-Mansour Seamount
977 Normal faults

Stage 1

b) Pliocene

Spain Málaga

Serrata Fault System

Cabo de Gata

Eastern Alboran Sea Basin

Andalucia A-1 Strike-slip faults

Reverse faults & later folds (Stages 1 and 2)

Western Alboran Sea Basin

976 No evidence for faulting

Alboran Ridge

978
Al-Mansour Seamount
977

Strait of Gibraltar

Tunis

Normal faults (Stage 1)
Folds (Stage 2)

Stage 1

Stage 2

c) Pleistocene

Spain Málaga

Serrata Fault System

Cabo de Gata

Eastern Alboran Sea Basin

Andalucia A-1 Strike-slip faults

Western Alboran Sea Basin

976 No evidence for faulting

Alboran Ridge

978 Folds
Al-Mansour Seamount
977

Strait of Gibraltar

Tunis

Folds (Stage 2)
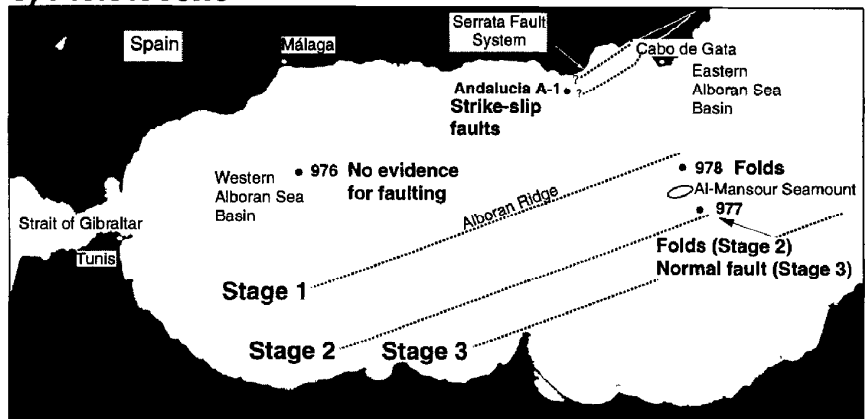Normal fault (Stage 3)

Stage 1

Stage 2 Stage 3

Fig. 13. Tectonic evolution of the Alboran Sea basin based on interpretation from seismic reflection data presented in the study. (a), (b) and (c) correspond to the description of structural features near well sites in the Miocene, Pliocene and Pleistocene, respectively. Dashed lines show the inferred axis of the delamination front at Stage 1 (Late Miocene–early Early Pliocene), Stage 2 (early Early Pliocene–Pleistocene), and Stage 3 (Pleistocene–Recent).
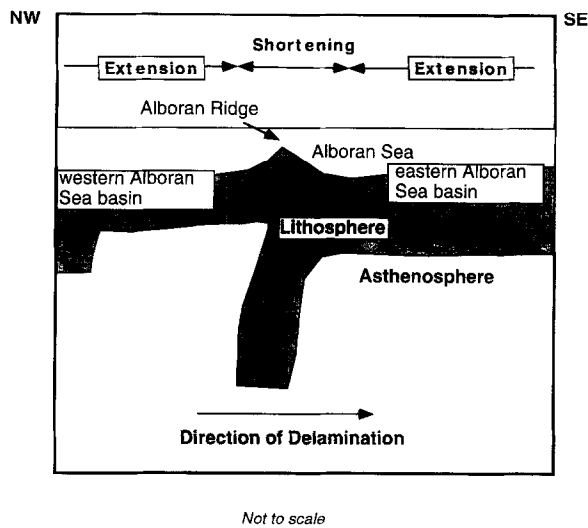
Fig. 14. Schematic model for the southeastward migration of delaminating lithosphere (Channell and Mareschal, 1989; Docherty and Banda, 1995).

occurring (Channell and Mareschal, 1989), as shown in Fig. 14. Docherty and Banda (1995) have also enunciated many supporting field observations for the model presented here (Fig. 14); such as the lack of evidence for oceanic crust being involved in the formation of the Alboran Sea basin and the oldest magmatic events found in the western part of Spain.

Based on our observations, we envision that the asymmetric evolution of the Alboran Sea basin occurs via lithospheric delamination in a southeasterly direction starting from the western Alboran Sea basin (Fig. 14). The majority of rifting caused by delamination in the western Alboran Sea basin ends in the Tortonian (Fig. 9). The migration of the delaminating lithosphere can be divided into three stages: (1) Stage 1 (Late Miocene–early Early Pliocene), (2) Stage 2 (early Early Pliocene–Pleistocene), and (3) Stage 3 (Pleistocene–Recent) based on mapping the extensional and compressional features in the Alboran Sea basin (Fig. 13). The boundary between Stage 2 and 3 is intra-Pleistocene. We surmise that the locus of delamination in the Late Miocene–early Pliocene (Stage 1) passed through the Alboran Ridge and Site 978 (Fig. 13a,b). The Alboran Ridge was under compression during Stage 1

(Chalouan et al., 1997) due to delamination. In the early Early Pliocene–Pleistocene (Stage 2), the locus of delamination moved through Site 977 (Fig. 13b,c). In the Pleistocene–Recent (Stage 3), this delamination front moves past Site 977 (Fig. 13c). Between Stages 1 and 2, the rate of migration of the delamination front in the Alboran Sea basin is estimated to range between the orders of millimeters–centimeters/year. If we estimate the time bracketed by Stage 2 to be 3.5 My (mid-Zanclean to mid-Pleistocene) at most, and the distance travelled by the locus of delamination to be ~29.3 km (from Fig. 13), then the rate of delamination is 0.83 cm/yr. This assumes that the sediments during Stage 2 at Site 977 were folded shortly after the deposition (Fig. 10). Near Site 977, onlap features are only seen within Stage 3 (Pleistocene–Recent) sediments (Fig. 10). The rate of delamination could be higher if the time represented by Stage 2 is smaller. This agrees rather well with the estimates given by Bird and Baumgardner (1981) but Channell and Mareschal (1989) are unable to migrate the delamination front in their numerical modeling. Channell and Mareschal (1989) attribute that perhaps a steady-state convection in the asthenosphere is a necessary condition for the delamination front to move.

The delamination model presented alone does not explain the following observations:

(1) Apart from inferred southeasterly delamination in the Alboran Sea basin, strike-slip faulting has an overprint which is operating independently of the stress regime created by delamination. Changes in compression direction between Europe and Africa from the Tortonian onward (Montenat et al., 1987) oblique to the existing faulting will create strike-slip motion and pull-apart structures (Comas et al., 1992; Maldonado et al., 1992; Watts et al., 1993). This will result in reorganizing the Alboran Sea basin (Comas et al., 1992; Maldonado et al., 1992; Watts et al., 1993). We also notice strike-slip motion in the northern Alboran Sea basin from the Late Miocene onwards.

(2) Near Site 978 we do not see any evidence for change from compressional to extensional regime as we would infer when the delamina-

tion front moves towards Site 977. The start of Stage 3 should predict normal faulting near Site 978, contrary to our observations (Fig. 13).

(3) The southeasterly migrating delamination model alone does not explain the onset of compressional features in the Pliocene–Pleistocene noticed by other workers in the western Alboran Sea basin (Bourgois et al., 1992; Campillo et al., 1992).

The main line of evidence for a continental lithospheric detachment model (continental delamination or extensional collapse) is that within the Alboran Sea and Rif-Betic Mountains, a low velocity, aseismic and strongly attenuating layer (assumed to be an asthenospheric mantle) replaces a high velocity, seismically active layer (assumed to be a lithospheric mantle) between the depths of 20 and 60 km (Seber et al., 1996). Both continental delamination (Fig. 14) and extensional collapse should predict the replacement of lithospheric mantle by asthenospheric mantle manifested by high temperature, low pressure metamorphism (Platt et al., 1996). Seismicity deeper than 60 km, mostly present in the western Alboran Sea basin (Seber et al., 1996; Mezcua and Rueda, 1997), supports the hypothesis that the delamination is in a more mature stage in the west than in the east (Docherty and Banda, 1995). An active delamination model (Docherty and Banda, 1995; Comas et al., 1996; Seber et al., 1996) does not explain the occurrence of a deep earthquake in southern Spain (Grimison and Chen, 1986). Such a deep earthquake could be due to sinking of a detached oceanic lithosphere (Grimison and Chen, 1986) or a detached continental delaminated lithosphere (Mezcua and Rueda, 1997). A detached continental delaminated lithosphere (Mezcua and Rueda, 1997) would mean that the delamination process has stopped (Bird and Baumgardner, 1981) at present. The presence of asthenospheric mantle overlying lithospheric mantle at shallow depths (Fig. 14) beneath the Alboran Sea (Seber et al., 1996) would no longer exist if the delaminated continental lithosphere has broken off. Support for an extensional collapse hypothesis (Dewey, 1988; Platt and Vissers, 1989) is not present in our

results (Fig. 13). Extensional collapse should have resulted in rifting roughly coeval throughout the entire Alboran Sea basin (Docherty and Banda, 1995). The westward continental delamination model of Comas et al. (1996) predicts younger extensional features in the western part of the Alboran Sea basin, in contrast to our observations.

Docherty and Banda (1995) have speculated that the delamination could have occurred due to the offset in the thickening of the crust and the lithospheric mantle (Channell and Mareschal, 1989). In the late Paleogene, the thickened crust and lithospheric mantle at the site of the present day Alboran Sea were juxtaposed against Iberian and Maghrebian passive margins (Docherty and Banda, 1995). Passive margins with thin crust and thicker mantle lithosphere to the west would perhaps create the required asymmetry for the start of delamination in the Alboran Sea basin (Docherty and Banda, 1995). Delamination could also occur due to cracking, slumping or plume erosion in the lithospheric mantle going to the tip of the continental crust (Bird, 1979). Such a phenomena may cause the eruption of basalts and diatremes (Bird, 1979) but it would be hard to distinguish whether the occurrence of basalts and diatremes are due to the initial weakness causing delamination or is the effect of continental delamination as a whole. There is little evidence for crustal melting and magma generation in the western Alboran Sea (Docherty, pers. commun.). However, the presence of volcanoes in the western Alboran Sea basin has been interpreted from basement highs on the seismic reflection surveys (Chalouan et al., 1997). Possibly, the delamination is not occurring at the Moho beneath the Alboran Sea but within the lithospheric mantle, which is not in agreement with the numerical models (Bird, 1979; Channell and Mareschal, 1989). The basement at Site 976 has granitic melts formed at temperatures greater than 670°C (Platt et al., 1996). The third possibility for the initiation of delamination could be due to thickened lithospheric mantle with no thickening in the crust during convergence (Channell and Mareschal, 1989). Evidence for crustal thickening in the Alboran Sea (Platt et al., 1996) and inland Spain (Dewey, 1988; Platt and Vissers, 1989), manifested as high-pres-

sure metamorphism prior to the Alboran Sea basin formation, excludes such a possibility.

Our results (Fig. 13) can also be used as evidence for asynchronous evolution of the Alboran Sea basin via a rapidly retreating subduction zone (Malinverno and Ryan, 1986; Zeck et al., 1992; Royden, 1993). They too predict adjacent regions of compression and extension occurring at the same time within the basin (Fig. 13). Such models involve the presence of subducting oceanic lithosphere in the vicinity of the Alboran Sea (Malinverno and Ryan, 1986; Zeck et al., 1992; Royden, 1993). Apart from tomographic images of possible detached lithosphere trending SW–NE between 200 and 700 km depth below the Betic–Alboran area (Blanco and Spakman, 1993), there is no other collaborating evidence for Alboran Sea basin tectonics from the Late Miocene onwards being driven by an oceanic lithosphere (Grimison and Chen, 1986; Docherty and Banda, 1995). Royden (1993) advocates a presently active westward retreat of an easterly dipping subduction zone as a mechanism for the formation of Alboran Sea basin and the Gibraltar Arc. The model of Royden (1993) predicts that ancestral morphological features within the Alboran Sea basin were arcuate in shape, similar to the thrust sheets along the Strait of Gibraltar and younger extensional features found in the western part of the basin. Rather, we notice a linear, NE–SW trending Alboran Ridge dividing the Alboran Sea basin (Fig. 1). If the westward retreating subduction is still active today (Royden, 1993) in the Gulf of Cadiz (west of Strait of Gibraltar), then earthquakes should indicate an eastward-dipping Benioff zone. Support for such a Benioff zone is not present in the Gulf of Cadiz (Seber et al., 1996; Mezcua and Rueda, 1997). A 640 km deep earthquake beneath southern Spain is assumed to be caused by the sinking of a detached oceanic lithosphere instead of an active subduction process (Grimison and Chen, 1986).

11. Conclusions

We have successfully correlated biostratigraphic data to seismic reflection data in different parts of the Alboran Sea basin using synthetic seismograms. The ODP Leg 161 data has allowed separate well-to-seismic correlation within the eastern and western Alboran Sea basin for the first time. Possible uncertainties in the well-to-seismic correlation using ODP Leg 161 laboratory data will not affect our geological conclusions. The three main conclusions of our study (Fig. 13) are as follows:

(1) Extension ended in the Late Miocene in the western Alboran Sea basin but continued until the Early Pliocene in parts of the eastern Alboran Sea basin. There is also evidence for recent normal faulting in the Eastern Alboran Sea basin.

(2) Adjacent extension and compression have occurred in the Alboran Sea basin from the Miocene to Recent. We surmise that the delamination front passed through the Alboran Ridge and Site 978 in the Late Miocene–Early Pliocene (Stage 1 in Fig. 13). Perhaps this delamination front has migrated further southeastward (stages 2 and 3 in Fig. 13) at a rate ranging from a few millimeters to a few centimeters per year.

(3) In the northern Alboran Sea basin, we find evidence for strike-slip fault systems extending from present-day inland Spain offshore to the Alboran Sea, affecting Late Miocene sediments. We believe that we are noticing first order features predicted by a southeasterly delamination model for the formation of the Alboran Sea basin. However, effects of delamination are overprinted by strike-slip faulting within the Alboran Sea basin, caused by convergence of the African and Eurasian plates.

Our model is based on limited observations made on the timing of structural activity in different parts of the Alboran Sea basin. The future direction for this study is the development of regional isopach maps from the Miocene–Recent reflectors (Table 1) delineated by the synthetic seismogram work conducted here. Isopach maps using thousands of kilometers of multi-channel seismic data will provide additional tests for the different hypotheses on the development of the Alboran Sea basin.

Acknowledgements

References

Biddle, K.T., Christie-Blick, N., 1989. Glossary — strike-slip deformation, basin formation, and sedimentation. In: Foster, N.H., Beaumont, E.A. (Eds.), Structural Concepts and Techniques II, Basement-Involved Deformation, Treatise of Petroleum Geology, Reprint Series No. 10. Tulsa, Okla., pp. 273–284.

Bird, P., 1979. Continental delamination and the Colorado Plateau. J. Geophys. Res. 84, 7561–7571.

Bird, P., Baumgardner, J., 1981. Steady propagation of delamination events. J. Geophys. Res. 86, 4891–4903.

Blanco, M.J., Spakman, W., 1993. The P-wave velocity structure of the mantle below the Iberian Peninsula: Evidence for subducted lithosphere below southern Spain. Tectonophysics 221, 13–34.

Bourgois, J., Mauffret, A., Ammar, A., Demnati, A., 1992. Multichannel seismic data imaging of inversion tectonics of the Alboran Ridge (Western Mediterranean Sea). Geo-Mar. Lett. 12, 117–122.

Campillo, A.C., Maldonado, A., Mauffret, A., 1992. Stratigraphic and tectonic evolution of the Western Alboran Sea: Late Miocene to Recent. Geo-Mar. Lett. 12, 165–172.

Chalouan, A., Rachida, S., Michard, A., Bally, A.W., 1997. Neogene tectonic evolution of the southwestern Alboran Basin as inferred from seismic data off Morocco. Am. Assoc. Pet. Geol. Bull. 81, 1161–1184.

Channell, J.E.T., Mareschal, J.C., 1989. Delamination and asymmetric lithospheric thickening in the development of the Tyrrhenian Rift, In: Coward, M. (Ed.), Alpine Tectonics. Spec. Publ. Geol. Soc. London 45, 285–300.

Comas, M.C., Garcia-Dueñas, V., Jurado, M.J., 1992. Neogene tectonic evolution of the Alboran Sea from MCS Data. Geo-Mar. Lett. 12, 157–164.

Comas, M.C., Zahn, R., Klaus, A., et al., 1996. Proc. ODP Init. Repts. 161, 1023 pp.

De Galdeano, C.S., Vera, J.A., 1992. Stratigraphic record and paleogeographical context of the Neogene basins in the Betic Cordillera, Spain. Basin Res. 4, 21–36.

De Larouziere, F.D., Bolze, J., Bordet, P., Hernandez, J., Montenant, C., ott D' Estevou, P., 1988. The Betic segment of the lithospheric Trans-Alboran shear zone during the Late Miocene. Tectonophysics 152, 41–52.

Dewey, J.F., 1988. Extensional collapse of orogens. Tectonics 7, 1123–1139.

Docherty, J.I.C., Banda, E., 1992. A Note on the subsidence history of the northern margin of the Alboran Sea. Geo-Mar. Lett. 12, 82–87.

Docherty, J.I.C., Banda, E., 1995. Evidence for the eastward migration of the Alboran Sea based on the regional subsidence analysis: A case for basin formation by delamination of the subcrustal lithosphere. Tectonics 14, 804–818.

Fernandez, J.R., De Galdeano, C.S., 1992. Onshore Neogene stratigraphy in the north of the Alboran Sea (Betic Internal Zones): Paleogeographic implications. Geo-Mar. Lett. 12, 123–128.

Garcia-Dueñas, V., Martinez-Martinez, J.M., Navarro, F., 1989. La Zona de Falla de Torres Cartas, conjunto de fallos normales de Bajo Angulo entre Nevado-Filabrides y Alpujarrides (Sierra Alhamilla, Beticas Orientalos). Geogaceta 1, 17–18.

Gardner, G.H.F., Gardner, L.W., Gregory, A.R., 1974. Formation velocity and density — The diagnostic basics for stratigraphic traps. Geophysics 39, 770–780.

Gregory, A.R., 1977. Aspects of rock physics from laboratory and log data that are important to seismic interpretation. In: Payton, C.E. (Ed.), Seismic Stratigraphy — Applications to Hydrocarbon Exploration. Am. Assoc. Pet. Geol. Mem. 26, 15–46.

Grimison, N.L., Chen, W.-P., 1986. The Azores–Gibraltar plate boundary: Focal mechanisms, depths of earthquakes, and their tectonic implications. J. Geophys. Res. 91, 2029–2047.

Hamilton, E.L., 1976. Variation of density and porosity with depth in deep-sea sediments. J. Sediment. Petrol. 46, 280–300.

Hamilton, E.L., Bachman, R.T., 1982. Sound velocity and related properties of marine sediments. J. Acoust. Soc. Am. 72, 1891–1904.

Jurado, M.J., Comas, M.C., 1992. Well log interpretation and

seismic character of the Cenozoic sequence in the northern Alboran Sea. Geo-Mar. Lett. 12, 129–136.

Lambert, C., 1981. Andalousie A-1, Rapport Final Du Sondage, Elf Aquitaine, Madrid, Spain, 13 pp.

Lorenzo, J.M., Hesselbo, S., 1996. Seismic-to-well correlation of seismic unconformities at Leg 150 continental slope sites. Proc. ODP, Sci. Results 150, 293–307.

Maldonado, A., Comas, M.C., 1992. Geology and geophysics of the Alboran Sea. Geo-Mar. Lett. 12, 61–65.

Maldonado, A., Campillo, A.C., Mauffret, A., Alonso, B., Woodside, J., Campos, J., 1992. Alboran Sea Late Cenozoic tectonic and stratigraphic evolution. Geo-Mar. Lett. 12, 179–186.

Malinverno, A., Ryan, B., 1986. Extension in the Tyrrhenian Sea and shortening in the Apennines as a result of arc migration driven by sinking of the lithosphere. Tectonics 5, 227–245.

Mauffret, A., El-Robrini, M., Gennesseaux, M., 1987. Indice de la compression Recente en Mer Mediterranee: Un basin losangique sur la marge Nord-Algerienne. Bull. Soc. Geol. Fr. 3, 1195–1206.

Mezcua, J., Rueda, J., 1997. Seismological evidence for a delamination process in the lithosphere under the Alboran Sea. Geophys. J. Int. 129, F1–F8.

Mitchum Jr., R.M., Vail, P.R., Thompson, S., , III1977. The depositional sequence as a basic unit for stratigraphic analysis. In: Payton, C.E. (Ed.), Seismic Stratigraphy — Applications to Hydrocarbon Exploration. Am. Assoc. Pet. Geol. Mem. 26, 53–62.

Montenat, C., Ott d'Estevou, P., Masse, P., 1987. Tectonic–sedimentary characters of the Betic Neogene basins evolving in a crustal transcurrent shear zone (SE Spain). Bull. Cent. Rech. Explor. Prod. Elf Aquitaine 11, 1–22.

Peterson, R.A., Fillipone, W.R., Coker, E.B., 1955. The synthesis of seismograms from well log data. Geophysics 20, 516

Platt, J.P., Vissers, R.L.M., 1989. Extensional collapse of thickened continental lithosphere: A working hypothesis for the Alboran Sea and Gibraltar Arc. Geology 17, 540–543.

Platt, J.P., Soto, J.I., Comas, M.C., Leg 161 Shipboard Scientists, 1996. Decompression and high-temperature–low-pressure metamorphism in the exhumed floor of an extensional basin, Alboran Sea, Western Mediterranean. Geology 24, 447–450.

Royden, L.H., 1993. Evolution of retreating subduction boundaries formed during continental collision. Tectonics 12, 629–638.

Seber, D., Barazangi, M., Ibenbrahim, A., Demnati, A., 1996. Geophysical evidence for lithosphere delamination beneath the Alboran Sea and Rif-Betic Mountains. Nature 379, 785–790.

Sheriff, R.E., 1977. Limitations on resolution of seismic reflections and geologic detail derivable from them. In: Payton, C.E. (Ed.), Seismic Stratigraphy — Applications to Hydrocarbon Exploration. Am. Assoc. Pet. Geol. Mem. 26, 3–14.

Sheriff, R.E., 1981. Encyclopedic Dictionary of Exploration Geophysics. Society of Exploration Geophysics, Tulsa, Okla, 266 pp.

Watts, A.B., Platt, J.P., Buhl, P., 1993. Tectonic evolution of the Alboran Sea Basin. Basin Res. 5, 153–177.

Woodside, J.M., Maldonado, A., 1992. Styles of compressional neotectonics in the eastern Alboran Sea. Geo-Mar. Lett. 12, 111–116.

Zeck, H.P., Monie, P., Villa, I.M., Hansen, B.T., 1992. Very high rates of cooling and uplift in the Alpine Belt of the Betic Cordilleras, Southern Spain. Geology 20, 79–82.